FBXO22 possesses both pro-tumorigenic and anti-metastatic roles in breast cancer progression

Rui Sun[1], Hong-Yan Xie[1-3], Jin-Xian Qian[1-3], Yan-Ni Huang[3-5], Fan Yang[3-5], Fang-Lin Zhang[1-3, *], Zhi-Min Shao[1-6, *], Da-Qiang Li[1-6, *]

[1]Shanghai Cancer Center and Institutes of Biomedical Sciences, Shanghai Medical College, Fudan University, Shanghai 200032, China

[2]Cancer Institute, Shanghai Medical College, Fudan University, Shanghai 200032, China

[3]Department of Oncology, Shanghai Medical College, Fudan University, Shanghai 200032, China

[4]Department of Breast Surgery, Shanghai Medical College, Fudan University, Shanghai 200032, China

[5]Key Laboratory of Breast Cancer in Shanghai, Shanghai Medical College, Fudan University, Shanghai 200032, China

[6]Key Laboratory of Medical Epigenetics and Metabolism, Shanghai Medical College, Fudan University, Shanghai 200032, China

*Correspondence:

Fang-Lin Zhang: zhangfanglin555@sina.com

Zhi-Min Shao: zhimingshao@yahoo.com

Da-Qiang Li: daqiangli1974@ fudan.edu.cn

Running title: Dual roles of FBXO22 in mammary tumorigenesis and metastasis

1

Conflict of interest statement

The authors declare no potential conflicts of interest.

Grant Support

Abbreviations

EMT, epithelial-mesenchymal transition; ER, estrogen receptor; FBXO22, F-box only protein 22; GSK3β, glycogen synthase kinase 3β; HER2, human epidermal growth receptor 2; PR, progesterone receptor; SCF, SKP1-Cullin-F-box protein; shRNA, short hairpin RNA; siRNA, small interfering RNA, TNBC, triple-negative breast cancer

Manuscript information

Words: 5500 (Introduction, Results, Discussion, and Figure Legends)

References: 44

Figures: 7

Supplementary Figures: 10

Supplementary Tables: 8

Abstract

The molecular underpinnings behind malignant progression of breast cancer from a localized lesion to an invasive and ultimately metastatic disease are incompletely understood. Here we report that F-box only protein 22 (FBXO22) plays a dual role in mammary tumorigenesis and metastasis. FBXO22 was upregulated in primary breast tumors and promoted cell proliferation and colony formation in vitro and xenograft tumorigenicity in vivo. Surprisingly, FBXO22 suppressed epithelial-mesenchymal transition (EMT), cell motility, and invasiveness in vitro and metastatic lung colonization in vivo. Clinical data showed that expression levels of FBXO22 were associated with favorable clinical outcomes, supporting the notion that metastasis, rather than primary cancer, is the major determinant of the mortality of breast cancer patients. Mechanistic investigations further revealed that FBXO22 elicits its antimetastatic effects by targeting SNAIL, a master regulator of EMT and breast cancer metastasis, for ubiquitin-mediated proteasomal degradation in a glycogen synthase kinase 3β (GSK3β) phosphorylation-dependent manner. Importantly, expression of SNAIL rescued FBXO22-mediated suppression of EMT, cell migration, and invasion. A patient-derived tryptophan-to-arginine mutation at residue 52 (W52R) within the F-box domain impaired FBXO22 binding to the SKP1-Cullin1 complex and blocked FBXO22-mediated SNAIL degradation, thus abrogating the ability of FBXO22 to suppress cell migration, invasion, and metastasis. Collectively, these findings uncover an unexpected dual role for FBXO22 in mammary tumorigenesis and metastatic progression and delineate the mechanism of an oncogenic mutation of FBXO22 in breast cancer progression.

Key words

3

Introduction

Malignant progression of breast cancer is a highly complex process involving primary tumor growth and invasion followed by metastatic dissemination to distant organs (1). Clinical evidence shows that the vast majority of breast cancer-related mortality occurs as a result of distant metastases rather than primary tumors themselves (2). To improve clinical outcomes, there is an urgent need to identify the molecular determinants governing breast cancer metastatic progression and novel therapeutic targets for antimetastatic therapy. Notably, breast cancer is a highly heterogeneous disease with distinct molecular subtypes and metastatic behaviors (3). According to the expression status of estrogen receptor (ER), progesterone receptor (PR), and human epidermal growth receptor 2 (HER2), breast cancer is clinically divided into three major molecular subtypes, including luminal, HER2-positive, and triple-negative breast cancer (TNBC) (3). Generally, luminal breast tumors tend to have low probability of metastatic spread with the best outcome, while HER2-positive and TNBC subtypes have higher propensity for metastatic progression and are associated with worse prognosis (4).

Considerable evidence suggests that aberrant activation of oncogenic epithelial-mesenchymal transition (EMT) program is implicated in breast cancer invasion and metastasis in both murine models and humans (5). EMT is characterized by the loss of epithelial characteristics and the acquisition of a mesenchymal phenotype with enhanced migratory and invasive properties (6). This phenotypic conversion is controlled by a network of transcription factors, including SNAIL (7,8), SLUG (9), ZEB1 (10), ZEB2 (11), and TWIST (12). Of them, SNAIL is uniquely required for EMT initiation by transcriptionally repressing E-cadherin expression (7,8,13). Consistently, elevated expression of SNAIL in mammary epithelial cells and primary breast tumors is sufficient to induce EMT and is correlated with increased metastasis, recurrence, and poorer clinical outcome (14-16). Given its clinical importance, an in-depth understanding of the

4

regulatory mechanisms of SNAIL may lead to novel therapeutic interventions for metastatic breast cancer. Recent work shows that SNAIL is a highly instable protein, which is regulated post-translationally by the ubiquitination machinery (16-18). However, the regulatory mechanism of SNAIL in breast cancer still remains elusive.

The ubiquitin-proteasome system controls ubiquitin-dependent proteolysis of critical regulatory proteins through a three-step enzymatic cascade, involving the ubiquitin-activating enzyme (E1), the ubiquitin-conjugating enzyme (E2), and the ubiquitin ligase (E3) (19). The largest family of E3 ubiquitin ligases in eukaryotes is the SKP1-Cullin-F-box protein (SCF) E3 ligase complex, which consists of four components, including an adaptor protein SKP1, a scaffold protein Cullin 1, a RING protein RBX1 or RBX2, and a F-box protein (20). The F-box protein component determines substrate specificity by binding to SKP1 and Cullin 1 through the F-box domain and to substrates through other protein-protein interaction motifs (21,22). The human genome encodes 69 F-box proteins, which can be classified into three families based on the presence of specific substrate recognition domains, including F-box and WD40 domain (FBXW), F-box and leucine-rich repeat (FBXL), and F-box and other domains (FBXO) (21,22). To date, the biological functions and physiological substrates for the vast majority of F-box proteins remain undefined. A case in point is F-box only protein 22 (FBXO22), a poorly characterized member of the F-box protein family. Available evidence shows that FBXO22 promotes hepatocellular carcinoma progression through mediating ubiquitin-dependent degradation of tumor suppressor krüppel-like factor 4 (KLF4) (23). In addition, FBXO22 regulates histone methylation marks and senescence through targeting lysine-specific demethylase 4A (KDM4A) (24) and p53 (25) for proteasomal degradation, respectively. However, the biological functions and molecular mechanisms of FBXO22 in breast cancer remain unexplored.

In the present study, we report that FBXO22 is upregulated in primary breast tumors and promotes breast cancer cell proliferation and xenograft tumor growth. Strikingly, FBXO22 suppresses EMT and breast cancer invasion and metastasis through glycogen synthase kinase 3β (GSK3β) phosphorylation-dependent degradation of SNAIL. More interestingly, we found that a patient-derived missense mutation within the F-box domain compromises the metastasis suppressive function of FBXO22 by protecting SNAIL from FBXO22-mediated degradation. These findings uncover a dual function of FBXO22 in the control of breast cancer growth and metastasis and identify an oncogenic mutation of FBXO22 in breast cancer progression through enhancing SNAIL stability.

Materials and methods

Cell culture and chemicals

All cell lines used in this study were obtained from the Type Culture Collection of the Chinese Academy of Sciences (Shanghai, China) and were authenticated by monitoring cell vitality, mycoplasma contamination, and short tandem repeat profiling. Cells were expanded and frozen immediately into numerous aliquots after arrival in 2014. MCF10A cells were cultured in DMEM/F12 supplemented with 5% donor horse serum, 10 µg/ml insulin, 20 ng/ml epidermal growth factor, 0.5 µg/ml hydrocortisone, and 100 ng/ml cholera toxin. SK-BR-3 and MDA-MB-231 cells were cultured in McCoy's 5A and Leibovitz's L-15 medium, respectively. Other cell lines were maintained in high-glucose DMEM medium. All media were supplemented with 10% fetal bovine serum (FBS). Culture media and supplements were obtained from BasalMedia (Shanghai, China). Horse serum and FBS were from Gibco (Carlsbad, USA). All chemicals and regents were purchased from Sigma-Aldrich (St. Louis, USA) unless otherwise noted. GSK3β inhibitor CHIR-99021, PKA inhibitor H89, and PKD1 inhibitor CID755673 were obtained from Selleck Chemicals (Houston, USA).

Tissue samples

Primary breast tumor samples were collected from routine surgical operation at Fudan University Shanghai Cancer Center. Characterization of clincopathological features of 164 primary breast cancer patients is present in **Supplementary Table S1**. All samples were obtained with informed consent and approved by the hospital institutional review board. This study was conducted in accordance with the ethical guidelines of the Declaration of Helsinki.

DNA constructs, transfection, and viral transduction

Myc-DDK-FBXO22, Myc-DDK-SNAIL, and short hairpin RNAs (shRNAs) targeting human FBXO22 (shFBXO22) were purchased from Origene (Rockville, USA). Small interfering RNA

7

(siRNA) targeting GSK3β (siGSK3β) and nontargeting negative control (siNC) were purchased form GenePharma (Shanghai, China) (**Supplementary Table S2**). To generate HA-FBXO22 and Flag-SNAIL constructs, FBXO22 and SNAIL cDNAs were amplified by PCR and subcloned into the lentiviral vector pCDH-CMV-MCS-EF1-Puro (System Biosciences, Mountain View, USA). To generate various HA-FBXO22 deletion truncations, FBXO22 cDNA was amplified by PCR and cloned into the pCDH-CMV-MCS-EF1-Puro. To generate various GST-FBXO22 and GST-SNAIL deletion constructs, FBXO22 and SNAIL cDNAs were amplified by PCR and then subcloned into pGEX-6P-1 expression vector (kindly provided by Yanhui Xu, Fudan University, Shanghai, China). Site directed mutagenesis HA-FBXO22 mutant (W52R) and Flag-SNAIL S4A mutant (S107A, S111A, S115A, and S119A) were generated using a QickChange II XL Site-Directed Mutagenesis Kit (Stratagene, La Jolla, USA). All constructs were verified by sequence analysis (HuaGene Biotech, Shanghai, China). All primers used for molecular cloning are listed in **Supplementary Tables S3 and S4**.

Transient plasmid transfection was carried out using Neofect (Tengyi Biotech, Shanghai, China) or Lipofectamine 2000 (Invitrogen, Waltham, USA) DNA transfection reagents according to the manufacturer's protocol. To generate stable cell lines expressing shRNAs or cDNAs, HEK293T cells were transfected with each lentivirus expression vector and packaging plasmid mix using Neofect DNA transfection reagents. The supernatant containing viruses was collected 48 h after transfection, filtered, and used for infecting target cells in the presence of 8 μg/ml of polybrene prior to drug selection with 2 μg/ml of puromycin for one week. SiRNA transfection was performed using Lipofectamine RNAiMAX (Invitrogen). The efficiency of silencing was assessed by immunoblotting 60 h after transfection.

Antibodies, immunoblotting, immunoprecipitation, immunohistochemistry, and Immunofluorescence

8

Detailed information for primary antibodies is provided in **Supplementary Table S5**. All of secondary antibodies for immunoblotting and immunofluorescent analysis were obtained from Cell Signaling Technology (Danvers, USA).

For immunoblotting analysis, cells were lysed in modified RIPA buffer (50 mM Tris-HCl, pH7.4, 1% Nonidet P-40, 0.25% sodium deoxycholate, 150 mM NaCl, and 1 mM EDTA) supplemented with protease inhibitors and phosphatase inhibitors (Bimake, Houston, USA). Protein concentrations were determined using BCA protein assay reagent (Yeasen, Shanghai, China). Cellular extracts were resolved by SDS-PAGE, transferred to PVDF membranes (Millipore, Billerica, USA), and incubated with the indicated primary antibodies. Corresponding antibody specific signals were detected using enhanced chemiluminescent substrate kit (Yeasen).

To immunoprecipitate exogenously expressed and endogenous proteins, cell extracts were incubated with primary antibodies or control IgG in a rotating incubator overnight at 4°C, followed by incubation with protein A/G magnetic beads (Bimake) for another 2 h. The immunoprecipitates were washed three times with lysis buffer and analyzed by immunoblotting.

Immunohistochemistry (IHC) staining was carried out using EnVision Detection Systems Peroxidase/DAB (DAKO, Shanghai, China) following the manufacturer's recommendations. For each sample, semiquantitative H-scoring assessment was performed by multiplying staining intensity (0, negative; 1+, weak; 2+, moderate; and 3+, strong) with the percentage of positive cells (0–100%)(26). A minimum of 100 cells were evaluated in calculating the H-score. The final scores ranged from 0 to 300. Based on the receiver operating characteristic (ROC) curve analysis (27), the cutoff value for FBXO22 high expression was defined when the H score was more than 230. Interpretation of IHC results were performed by two independent scientists blinded to the corresponding clinicopathological data.

9

For indirect immunofluorescent staining, cells were washed three times in PBS, fixed in 4% paraformaldehyde, permeabilized in 0.1% Triton X-100 on ice, and blocked in 10% normal goat serum in PBST. Cells were incubated with primary antibodies overnight, washed three times in PBST, and incubated with the appropriate secondary antibody conjugated with 555-Alexa (red) or 488-Alexa (green), respectively. DNA staining was performed using fluoroshield mounting medium with DAPI (Abcam, Shanghai, China). Microscopic analyses were performed using a Leica SP5 confocal laser scanning microscopy (Leica Microsystems, Buffalo Grove, USA).

Quantitative real-time PCR (qPCR)

Total RNA was isolated using TRIzol reagent (Invitrogen) and then transcribed into cDNA using PrimeScript RT Master Mix (Takara, Dalian, China) according to the manufacture's protocol. qPCR was performed using the iQ SYBR Green Supermix (Bio-Rad Laboratories, Hercules, USA) on an Eppendorf Mastercycleer ep realplex4 instrument (Eppendorf, Germany). All oligonucleotide primers were synthesized in HuaGene Biotech. The values for specific genes were normalized to β-actin housekeeping controls, and data was present as mean ± standard deviations. All primers used for qPCR assays are listed in **Supplementary Table S6**.

***In vitro* and *in vivo* ubiquitination assays and analysis of the half-life of proteins**

In vivo ubiquitination assays were carried out as described previously (28). To carry out *in vitro* ubiquitination assay, HA-FBXO22 was expressed in HEK293T cells and immunopurified using anti-HA agarose beads (Bimake), and eluted with 3×HA peptide (GenScript, Nanjing, China). Flag-SNAIL was pulled down from transfected HEK293T cells using anti-Flag M2 beads (Sigma) as a substrate. The reaction was performed at 37°C for 1 h in 50 µL reaction buffer (Boston Biochem, Cambridge, USA) in the presence of ubiquitin, E1, E2 (UbcH5b), ATP, substrate and

10

purified E3. Polyubiquitinated SNAIL was resolved by SDS-PAGE and detected by immunoblotting with an anti-ubiquitin antibody. For assessing the half-life of proteins, cells were treated with 100 μg/mL cycloheximide (CHX) and then harvested at indicated time points for immunoblotting analysis. The densitometry of Western blots was quantified using ImageJ 1.50 processing software.

GST pull-down assay

The GST fusion proteins were expressed in *Escherichia coli* stain BL21 (Tiangen Biotech, Shanghai, China) and purified using the glutathione-agarose beads (GE Healthcare, Chicago, USA) according to the manufacturer's standard procedures. The empty vector (pGEX-6p-1) expressing GST alone was used as a negative control. GST fusion proteins were incubated with total cellular lysates of HEK293T cells expressing the indicated expression vectors. After 2 h incubation, beads were collected by centrifugation and washed five times to remove nonspecific binding. Bound proteins were resolved by SDS-PAGE and analyzed by immunoblotting with the indicated antibodies.

Cell viability, colony-formation, anchorage-independent growth, cell migration, and invasion assays

Cells were seeded in 96-well plates (2000 cells/well) in triplicate and cell viability was examined by Cell Counting Kit-8 (CCK-8) assay (Dojindo Laboratories, Kumamoto, Japan). For colony-formation assay, cells were seeded in 6-well plates (2000 cells/well) in triplicate and cultured under normal growth conditions for two weeks. Colonies were washed three times in PBS, fixed in methanol, stained with 0.1% crystal violet, and counted using an inverted microscope. To examine anchorage-independent 3D growth, MDA-MB-231 cells stably expressing pCDH and HA-FBXO22 (500 cells in 2 ml media) were seeded on 24-well ultra-low attachment surface plates (Corning, New York, USA) as described previously (29). After 2 weeks of culture, cells

11

were observed and counted under a phase-contrast microscopy. For wound-healing assay, cells were seeded in 6-well plates. When cells grown to confluence, the wound was created by 1 ml tips, the floated cells were removed through PBS washing, and the culture medium were replaced by medium containing 0.1% FBS. Images were taken at the indicated time points and the wound closure ratios were calculated. Migration and invasion assays were performed using the transwell chambers in the absence (migration) and presence (invasion) of growth factor-reduced Matrigel (Corning). Briefly, 5×10^4 cells in FBS-free medium were plated in the top chamber. Growth medium containing 10% FBS was used as a chemoattractant in the lower chamber. After indicated times, migrated and invaded cells were fixed and stained with 0.1% crystal violet. Cells were counted under an inverted microscope at 100× magnification.

In vivo tumor growth and experimental pulmonary metastasis assay

For subcutaneous inoculation, a total of 3×10^6 cells in 300 µl PBS were injected subcutaneously into the mammary fat pad of 6-week-old BALB/c female nude mice (Shanghai Cancer Institute, Shanghai, China). The tumors were measured every 7 days after injection and the tumor volume was calculated by the formula (length×width^2)/2. The mice were sacrificed 8 weeks after inoculation, and the removed tumors were subjected to HE staining. For experimental pulmonary metastasis assay, cells (2×10^6 in 200 µl PBS) were injected into tail veins of 6-week-old BALB/c female nude mice. Mice were sacrificed 6 weeks after injection. Lungs were removed and metastatic nodules were counted microscopically. In addition, paraffin-embedded lung tissue sections were stained by hematoxylin-eosin to examine the presence of micrometastases. All animal experiments were approved by Institutional Animal Care and Use Committee of Fudan University and animal care was in accordance with institutional guidelines.

Statistical analysis

All data are presented as the mean ± standard error from at least three independent experiments. The Student's *t*-test was used to compare data between two groups. Survival curves were obtained using the Kaplan-Meier method, and the log-rank test was used to test the difference in survival curves. Multivariate analysis was performed using the Cox's regression multiple hazard model. *P* values of less than 0.05 were considered statistically significant.

13

Results

FBXO22 enhances cell proliferation *in vitro* and tumor growth *in vivo*

To investigate the potential roles of FBXO22 in breast cancer, we first examined the expression levels of FBXO22 in 9 pairs of human breast tumor specimens and matched normal breast tissues by immunoblotting. Results showed that FBXO22 protein was upregulated in 7 out of 9 (77.8%) primary breast tumor tissues as compared with their normal counterparts (**Figure 1A**). Next, we determined the expression levels of FBXO22 in two normal human mammary epithelial cell lines and seven well-characterized breast cancer cell lines. As shown in **Figure 1B**, luminal-type breast cancer cell lines (MCF-7, T47D, and ZR-75-1) expressed relatively high levels of FBXO22 as compared with normal mammary epithelial cell lines (MCF10A and HBL100) as well as HER2-positive (SK-BR-3 and BT474) and TNBC (MDA-MB-231 and Hs578T) cell lines (30). These results suggest that FBXO22 is upregulated in human breast cancer tissues and poorly invasive luminal breast cancer cell lines.

To investigate the impact of FBXO22 on malignant phenotypes of breast cancer cells, we stably expressed FBXO22 in MCF10A, HBL100, MDA-MB-231, and Hs578T cells by lentiviral infection (**Figure 1C and Supplementary Figure S1A**). Cell proliferation assays using CCK-8 kit revealed that overexpression of FBXO22 accelerated cell proliferation in MDA-MB-231 and Hs578T cells (**Figure 1D and Supplementary Figure S1B**), but not in MCF10A and HBL100 cells (**Supplementary Figure S1C**). Colony growth assays demonstrated that expression of FBXO22 increased colony formation of MDA-MB-231 and Hs578T cells (**Figure 1E and Supplementary Figure S1D**). Anchorage-independent 3D growth assays (29) showed that overexpression of FBXO22 in MDA-MB-231 cells increased the size but not number of formed spheroidal clumps (**Supplementary Figure S1E and S1F**). In contrast, knockdown of FBXO22 in MCF-7 and ZR-75-1 cells using shFBXO22 (**Figure 1F** and **Supplementary Figure S1G**)

14

decreased cell viability (**Figure 1G**) and clonogenicity (**Figure 1H and Supplementary Figure S1H**).

To investigate whether FBXO22 could promote tumorigenic capacity of breast cancer cells *in vivo*, MDA-MB-231 cells stably expressing pCDH and HA-FBXO22 were subcutaneously injected into mammary fat pads of 6-week-old BALB/c nude mice. Consistent with *in vitro* results, xenograft tumors expressing HA-FBXO22 grew faster than those expressing empty vector (**Figure 1I-1K**). These results were confirmed by repeated experiments using newly established stable MDA-MB-231 cells expressing pCDH and HA-FBXO22 (**Supplementary Figure S2A-S2D**). Together, these results suggest that FBXO22 promotes breast cancer cell proliferation *in vitro* and tumor growth *in vivo*.

FBXO22 suppresses breast cancer cell migration, invasion, and metastasis

As an important hallmark of breast cancer cells is their ability to invade surrounding tissues and metastasize to distant organs (2), we next examined whether FBXO22 affects migratory and invasive properties of breast cancer cells *in vitro*. Wound-healing assays showed that expression of FBXO22 in MDA-MB-231 and Hs578T cells decreased wound closure rate compared to their control cells (**Figure 2A and 2B**). These results were further confirmed by Boyden's chamber migration assays (**Figure 2C and 2D**). Moreover, MDA-MB-231 and Hs578T cells stably expressing FBXO22 showed a less degree of invasion through Matrigel-coated invasion chambers (**Figure 2E and 2F**). Interestingly, overexpression of FBXO22 in MCF10A and HBL100 cells also decreased their migratory and invasive potential (**Supplementary Figure S3A-S3D**). In contrast, knockdown of FBXO22 by shFBXO22 in MCF-7 and ZR-75-1 cells enhanced their migratory and invasive capacity (**Figure 2G-2J and Supplementary Figure S3E and S3F**).

15

To address whether FBXO22 affects breast cancer metastasis *in vivo*, MDA-MB-231 cells stably expressing pCDH and HA-FBXO22 were injected into nude mice through the tail vein. As shown in **Figure 2K and 2L**, MDA-MB-231 cells expressing FBXO22 decreased the number of metastatic tumors in the lungs of nude mice. These results were supported by H.E. staining of lung sections of these mice (**Figure 2M**). Together, these results indicate that FBXO22 suppresses breast cancer cell migratory and invasive behaviors *in vitro* and lung metastatic potential *in vivo*.

Association of FBXO22 expression with clinical outcome of breast cancer patients

To determine the clinical significance of FBXO22 expression in patients with breast cancer, we analyzed FBXO22 expression levels by IHC on a tissue microarray containing 164 breast cancer samples with clinical fellow-up information (**Figure 3A**). Semiquantitative analysis showed that high expression of FBXO22 was observed in 34.7% (57/164) of patients, while 65.3% (107/164) of patients had FBXO22 low expression (**Supplementary Table S7**). Moreover, the expression levels of FBXO22 were associated with lymph node involvement, tumor grade, ER, PR, and HER2 expression status, and molecular subtypes (**Supplementary Table S7**). However, there is no statistical difference between FBXO22 expression levels and tumor size and TNM stage. This may be due to the limited sample size and only the early-stage of patients who were suitable for surgical treatment included in this study. Survival analysis using the Kaplan-Meier method revealed that patients with high FBXO22 expression had better overall survival (OS)(**Figure 3B**) and disease-free survival (DFS)(**Figure 3C**). Multivariate analysis showed that FBXO22 is an independent predictor for DFS (**Supplementary Table S8**). These results indicate that high expression levels of FBXO22 are associated with better prognosis of patients with breast cancer, supporting the notion that the main cause of death of breast cancer patients is not the primary tumor itself but the metastatic disease.

16

FBXO22 suppresses EMT by targeting SNAIL for proteasomal degradation

Despite remarkable advances in the treatment of primary breast tumors, metastasis to distant organs is a clinically daunting event accounting for over 90% of breast cancer-related mortality (2). Therefore, in the present study we focused on addressing the molecular mechanism by which FBXO22 suppresses breast cancer metastasis.

Accumulating evidence suggests that EMT plays a critical role in the process of breast cancer invasion and metastasis (31). The primary events of an EMT are the loss of epithelial markers (such as E-cadherin), accompanied by increased expression of mesenchymal markers (such as Vimentin) (6). To investigate whether FBXO22 regulates EMT, we stably expressed FBXO22 in MCF10A cell line, which expresses low levels of endogenous FBXO22 and has been widely used to study EMT (13). Immunoblotting analysis showed an upregulation of epithelial markers (E-cadherin, β-catenin, ZO-1, and Claudin-1) and a concomitant downregulation of mesenchymal markers (N-cadherin and Vimentin) in FBXO22-expressing cells (**Figure 4A**). qPCR analysis suggested that FBXO22 increased E-cadherin but decreased Vimentin mRNA levels (**Supplementary Figure S4A**). Immunofluorescent staining showed an increase in E-cadherin membrane staining in FBXO22-expressing cells as compared with control cells, whereas Vimentin exhibited a reverse trend (**Figure 4B**). Consistently, overexpression of FBXO22 downregulated Vimentin in mesenchymal-like MDA-MB-231 and Hs578T cells, while knockdown of FBXO22 downregulated E-cadherin in epithelial-like MCF-7 and ZR-75-1 cells (**Supplementary Figure S4B and S4C**). We next examined whether FBXO22 expression correlates with EMT markers in clinical breast tumor tissues. As E-cadherin expression is frequently reduced or absent in the great majority of invasive breast cancer due to promoter methylation or mutation (32,33), we examined expression levels of Vimentin in 164 breast cancer samples (**Supplementary Table S1**) by IHC. Interestingly, it was found that FBXO22

17

expression inversely correlates with Vimentin level in these clinical samples (**Supplementary Figure S4D and S4E**). These results suggest that FBXO22 suppresses EMT program.

EMT program is controlled by a network of transcription factors, including SNAIL, SLUG, ZEB1, ZEB2, and TWIST (7-12). To address the mechanism by which FBXO22 suppresses EMT, we next examined the effects of FBXO22 on expression levels of these EMT-inducing transcription factors. We found that overexpression of FBXO22 in MDA-MB-231 and Hs578T cells decreased SNAIL protein levels (**Figure 4C and Supplementary Figure S4B**). In contrast, knockdown of FBXO22 in MCF-7 and ZR-75-1 cells increased the protein levels of SNAIL (**Figure 4D and Supplementary Figure S4C**). In addition, overexpression or depletion of FBXO22 did not affect the expression levels of ZEB2 and TWIST (**Supplementary Figure S4B and S4C**). Moreover, overexpression of FBXO22 in MDA-MB-231 and Hs578T cells upregulated but not downregulated SLUG and differentially regulated ZEB1 (**Supplementary Figure S4B**). Based on these results, we reasoned that FBXO22 suppresses EMT program through, at least in part, negative regulation of SNAIL, which is uniquely required for EMT initiation (13,15).

In support of this notion, we noticed a downregulation of SNAIL in FBXO22-expressing xenograft tumors as compared with empty vector expressing controls (**Figure 4E**). Moreover, FBXO22 expression was inversely correlated with SNAIL in human breast cancer cell lines (**Figure 4F**). In contrast to a negative correlation between FBXO22 and SNAIL at protein level, induced expression of FBXO22 enhanced, while knockdown of FBXO22 reduced the mRNA levels of SNAIL (**Supplementary Figure S5A and S5B, respectively**). These results indicate that FBXO22 regulation of SNAIL occurs at post-transcriptional level. In agreement with these observations, FBXO22-mediated downregulation of SNAIL in MDA-MB-231 and Hs578T cells were effectively restored following treatment with 10 µM of proteasome inhibitor MG-132 for 6 h (**Figure 4G**), and knockdown of FBXO22 in MCF-7 and ZR-75-1 cells enhanced the half-life of

18

SNAIL protein (**Figure 4H and 4I**). These results suggest that FBXO22 targets SNAIL protein for proteasomal degradation.

Expression of SNAIL induces EMT in breast cancer cells by suppressing E-cadherin expression (7,8). To address whether SNAIL is indeed involved in FBXO22-mediated EMT, we stably expressed Flag-SNAIL alone or in combination with HA-FBXO22 in E-cadherin-expressing MCF-7 and T47D cells. As shown in **Figure 4J**, expression of SNAIL alone in both cell lines resulted in a reduction in E-cadherin expression. When HA-FBXO22 was co-expressed with Flag-SNAIL, reduced E-cadherin expression by SNAIL was effectively restored. These observations were further confirmed by immunofluorescent staining with an anti-E-cadherin antibody (**Figure 4K**). These results suggest that FBXO22 can block SNAIL-induced EMT program in human breast cancer cells.

FBXO22 interacts with SNAIL and promotes its polyubiquitination

To investigate the mechanism by which FBXO22 regulates SNAIL degradation, we next examined whether FBXO22 interacts with SNAIL. GST pull-down assays demonstrated that exogenously expressed Flag-SNAIL in HEK293T cells was able to interact with GST-FBXO22 but not GST control (**Figure 5A**). Reciprocally, exogenously expressed HA-FBXO22 interacted with GST-SNAIL (**Figure 5B**). To confirm these findings, HEK293T cells were transfected with HA-FBXO22 and Flag-SNAIL alone or in combination, and then subjected to reciprocal IP assays with an anti-Flag or anti-HA antibody. Immunoblotting analyses showed that HA-FBXO22 interacted with Flag-SNAIL when co-expressed (**Figure 5C**). Importantly, an interaction between FBXO22 and SNAIL at the endogenous protein levels was validated in ZR-75-1 and T47D cells by co-immunoprecipitation with an anti-SNAIL antibody (**Figure 5D**).

FBXO22 contains an N-terminal F-box domain and a C-terminal FIST_C (F-box and intracellular signal transduction, C-terminal) domain (**Supplementary Figure S6A**). To identify which region of FBXO22 is responsible for the interaction with SNAIL, we generated two GST-FBXO22 truncated constructs; a C-terminal deletion (amino acids 1-280) and an N-terminal deletion (amino acids 281-403) mutant. GST pull-down assays demonstrated that the C-terminal fragment of FBXO22 is required for its interaction with SNAIL (**Figure 5E and Supplementary Figure S6A**). SNAIL protein contains an N-terminal SNAG (SNAIL/Slug and Gfi-1) domain, a destruction (D) box in the middle, and four tandem zinc finger motifs in the C-terminus (16) (**Supplementary Figure S6B**). To identify the region in SNAIL that associates with FBXO22, we generated three deletion mutants of SNAIL, including a SNAG-domain deletion mutant (amino acids 76-264), a SNAG-domain and D-motif deletion mutant (amino acids 127-264), a C-terminal SNAIL (amino acids 154-264). GST pull-down assays demonstrated that the middle region (amino acids 127-153) of SNAIL is required for interacting with FBXO22 (**Figure 5F and Supplementary Figure S6B**).

As a major function of F-box proteins involves the ubiquitination of their target substrates (21,22), we next investigated whether FBXO22 could ubiquitinate SNAIL protein *in vivo*. To do this, HEK293T cells were transfected with Flag-SNAIL, V5-ubiquitin, and HA-FBXO22 alone or in combination. The sequential IP and immunoblotting analysis showed a significant increase of polyubiquitinated SNAIL protein in FBXO22 transfected cells under both native and denaturing conditions (**Figure 5G and 5H, respectively**). Moreover, overexpression of FBXO22 in MDA-MB-231 cells enhanced (**Figure 5I**), whereas knockdown of FBXO22 in MCF-7 cells decreased the ubiquitination levels of endogenous SNAIL (**Figure 5J**). *In vitro* ubiquitination assays demonstrated that FBXO22 significantly enhanced the ubiquitination levels of SNAIL in the presence of ubiquitin, E1, E2, and ATP (**Figure 5K**). These results suggest that FBXO22 ubiquitinates SNAIL *in vitro* and *in vivo*.

20

FBXO22 promotes SNAIL degradation in a GSK3β phosphorylation dependent manner

F-Box proteins generally recognize their substrates when they are phosphorylated (20). Previous studies have shown that SNAIL could be phosphorylated by GSK3β (16), protein kinase A (PKA) (34), and protein kinase D1 (PKD1) (17). To determine which signaling pathway is involved in FBXO22-mediated SNAIL degradation, MDA-MB-231 cells stably expressing pCDH and HA-FBXO22 were treated with or without GSK3β inhibitor CHIR-99021, PKA inhibitor H89, and PKD1 inhibitor CID755673. As shown in **Figure 6A**, CHIR-99021, but not H89 and CID755673, effectively blocked FBXO22-induced degradation of SNAIL. Consistently, knockdown of FBXO22 in MCF-7 cells led to an upregulation of SNAIL and this effect was further augmented by CHIR-99021 (**Figure 6B**). To rule out the off-target effects of CHIR-99021, MDA-MB-231 and Hs578T cells stably expressing pCDH and HA-FBXO22 were transfected with or without siGSK3β. As shown in **Supplementary Figure S7A**, depletion of GSK3β compromised FBXO22-mediated downregulation of SNAIL. Furthermore, treatment of cells with CHIR-99021 suppressed FBXO22-mediated ubiquitination of SNAIL (**Figure 6C**). These results suggest that FBXO22-mediated ubiquitination and degradation of SNAIL is GSK3β dependent.

Previous studies have shown that GSK3β phosphorylates SNAIL at serine (S) residues 107, 111, 115, and 119 (16). To examine whether these serine residues are required for the ubiquitination and degradation of SNAIL by FBXO22, we generated a mutant Flag-SNAIL expression vector in which S107, S111, S115, and S119 residues were mutated to alanine (hereafter referred to as S4A). As reported previously (16), Flag-SNAIL S4A predominantly localized to the nucleus and MG-132 treatment did not enhance its signal in the cytoplasm (**Supplementary Figure S7B**). Sequential IP and immunoblotting analyses showed that the ubiquitination levels of Flag-SNAIL S4A were reduced as compared with wild-type SNAIL in the presence of HA-FBXO22 (**Figure 6D**). Consistently, induced expression of FBXO22 resulted in

21

the degradation of wild-type SNAIL but not SNAIL S4A mutant (**Figure 6E**). CHX chase assays demonstrated that induced expression of FBXO22 resulted in a reduction in half-life of wild-type SNAIL but not S4A mutant (**Figure 6F and 6G**).

To determine whether FBXO22 suppresses breast cancer invasion metastasis through abrogating SNAIL-mediated oncogenic functions, we generated stable MDA-MB-231 cells expressing HA-FBXO22 alone or in combination with either Flag-SNAIL or Flag-SNAIL S4A by lentiviral infection. As shown in **Figure 6H and 6I**, induced expression of FBXO22 suppressed migration and invasion of MDA-MB-231 cells, and this effect was rescued by introduction of SNAIL, especially S4A mutant SNAIL. Together, these results demonstrate that FBXO22 mediates ubiquitination and degradation of SNAIL in a GSK3β phosphorylation-dependent manner and blocks SNAIL-mediated cell migration and invasion.

A patient-derived missense mutation within the F-box domain abrogates the ability of FBXO22 to degrade SNAIL and to suppress migration, invasion, and metastasis

The development of cancer is generally believed to require the accumulation of multiple genetic aberrations. To identify breast cancer related mutations in FBXO22, we analyzed the somatic mutation data from publicly available databases and identified a tryptophan to arginine mutation at residue 52 (W52R) within the F-box domain in a breast cancer patient (**Supplementary Figure S8A and S8B**). Moreover, the W52 residue of FBXO22 protein is highly conserved across a wide range of species (**Supplementary Figure S8C**).

As F-box domain is responsible for interacting with SKP1 and subsequent assembly of the SCF ligase complexes (21,22), we next examined whether the W52R mutation of FBXO22 affects its ability to bind to SKP1 and to regulate SNAIL proteolysis. To this end, we generated two variant HA-FBXO22 expression vectors encoding an F-box domain-deletion mutant (ΔF) and a W52R

mutant, respectively. Immunofluorescence staining showed that deletion of F-box domain (ΔF) or W52R mutation did not affect subcellular localization of FBXO22 (**Supplementary Figure S9A**). In contrast to wild-type FBXO22, ectopic expression of FBXO22 ΔF or W52R displayed an impaired ability to bind to SKP1 and Cullin 1 (**Figure 7A**) and to promote SNAIL degradation in MDA-MB-231 cells (**Figure 7B**). Furthermore, we found that wild-type FBXO22, but not either ΔF or W52R mutant, promoted SNAIL ubiquitination (**Figure 7C and 7D**). Consistently, expression of FBXO22 ΔF or W52R mutant enhanced the half-live of SNAIL as compared with its wild-type counterpart (**Figure 7E and Supplementary Figure S9B**). These results suggest that FBXO22 ligase activity is dependent on the integrity of F-box domain.

To define the roles of F-box motif-defective mutants in breast cancer invasion and metastasis, we established stable MDA-MB-231 cell lines expressing pCDH, FBXO22, FBXO22 ΔF, and FBXO22 W52R. *In vitro* cell migration and invasion assays (**Figure 7F and 7G**) and *in vivo* experimental lung metastasis assays (**Figure 7H-7J**) demonstrate that ectopic expression of FBXO22-ΔF and FBXO22 W52R compromised the ability of FBXO22 to suppress migratory, invasive, and metastatic potential of MDA-MB-231 cells compared to wild-type FBXO22. These results suggest that FBXO22 W52R mutation may contribute to breast cancer progression and metastasis through preventing SNAIL from FBXO22-mediated degradation (**Supplementary Figure S10**).

Discussion

In this study, we present several unexpected findings concerning the important but complex roles for FBXO22 in malignant progression of breast cancer.

First, FBXO22 plays both pro-tumorigenic and anti-metastatic roles in breast cancer progression. Among the identified 69 F-box proteins, extensive studies have been focused on a handful of F-box proteins, such as FBXW1, FBXW7, FBXW11, and FBXL1 (21). In this context, FBXW7 functions as a putative tumor suppressor (35), whereas FBXL1 exerts predominant oncogenic functions (36). In contrast, FBXW1 and FBXW11 exhibit context-dependent oncogenic or tumor-suppressive properties (21). To date, the majority of F-box proteins remain functionally mysterious with no established substrates (21). Here, we report that FBXO22 has a dual role in the process of malignant progression of breast cancer. In support of our results, a few of cancer-relevant signaling molecules have been shown to exert dual roles in cancer development and progression. For example, the Ski-related novel protein N (SnoN), a negative regulator of transforming growth factor β signaling, has been shown to promote mammalian tumorigenesis but inhibit EMT and tumor metastasis (37). Proto-oncogene MYC is overexpressed in 25% of human breast cancers and elicits malignant tumors in experimental animals (38). On the other hand, elevated expression of MYC suppresses breast cancer invasion and metastasis (39). Similarly, expression of Myc-associated zinc finger protein (MAZ) in basal-like breast cancer cells promotes proliferation but suppresses progression (40). Based on these results (37-40), we proposed that FBXO22 may help to establish the primary tumor colonies at the early stages of tumorigenesis by enhancing tumor cell viability and growth. When primary tumors progress to invasion and metastasis, FBXO22 expression may be suppressed through yet undefined mechanisms, thus allowing tumor cells to undergo EMT, invade, and metastasize. Although FBXO22 expression is elevated in primary breast tumors (**Figure 1**) and the SCF ubiquitin ligase has been proposed as a potential therapeutic target for human cancer

24

(41), our findings argue against direct targeting of FBXO22 as this may enhance metastatic capacity of breast cancer cells.

Second, FBXO22 is a new regulator of EMT in breast cancer progression through targeting SNAIL for ubiquitin-dependent proteasomal degradation in a GSK3β phosphorylation dependent manner. Emerging evidence shows that three F-box proteins, including FBXW1 (16), FBXL14 (18), and FBXO11 (17), are implicated in SNAIL ubiquitination and degradation. In this context, FBXW1 induces proteasomal degradation of SNAIL upon phosphorylation by GSK3β (16). In contrast, FBXL14 promotes proteasome degradation of SNAIL during hypoxia independently of phosphorylation by GSK3β (18). In addition, FBXO11 targets SNAIL for ubiquitination and degradation in a PKD1 phosphorylation-dependent manner (17). In this study, we found that FBXO22 enables to blocks SNAIL-mediated EMT (**Figure 4**). Mechanistic investigates further revealed that FBXO22 targets SNAIL for ubiquitination and subsequent degradation in a GSK3β phosphorylation dependent manner (**Figure 5 and 6**). Moreover, expression of SNAIL effectively rescues FBXO22-mediated suppression of breast cancer migration and invasion. These results suggest that FBXO22 exerts its metastasis-suppressive functions through blocking SNAIL-mediated EMT program.

Third, a cancer-associated W52 mutation within the F-box domain of FBXO22 is a functional mutation in breast cancer progression through blocking SNAIL degradation. Mutations of F-box proteins have been documented in human cancers. For instance, approximately 6% of human tumors harbored mutations in FBXW7 (35). Mutations in FBXO4 contribute to cyclin D1 overexpression in human cancer (42). In addition, FBXO11 is mutated in 4% of primary diffuse large B-cell lymphomas and tumor-derived mutants have impaired abilities to induce degradation of oncoprotein BCL6 (43). During analysis of breast cancer-related mutations in FBXO22, we found a highly conserved W52R mutation within the F-box domain. A serial of

25

biochemical assays demonstrated that the W52R mutation has impaired ability to assemble of the SCF ligase complex and to ubiquitinate SNAIL, thus protecting SNAIL from ubiquitin-mediated proteolysis by FBXO22. Consequently, *in vitro* and *in vivo* functional experiments further demonstrated that the W52R mutation compromises the ability of FBXO22 to suppress breast cancer migration, invasion, and metastasis (**Figure 7**). In addition, mutations of F-box proteins have been linked with therapeutic response (44). Thus, whether the W52R mutation of FBXO22 affects the sensitivity of breast cancer cells to conventional therapeutic agents remains to be investigated in the near future.

In summary, findings presented here showed that FBXO22 plays both pro-tumorigenic and anti-metastatic roles in breast cancer progression, and exerts its metastasis-suppressive functions through GSK3β phosphorylation-dependent degradation of SNAIL. Importantly, a patient-derived W52R mutation within the F-box motif abrogates the ability of FBXO22 to degrade SNAIL, thus promoting breast cancer invasion and metastasis (**Supplementary Figure S10**). These new findings provide mechanistic insights into the functional role for FBXO22 in regulating breast cancer development and progression and are clinically relevant.

26

References

1. Huber MA, Azoitei N, Baumann B, Grunert S, Sommer A, Pehamberger H, *et al.* NF-kappaB is essential for epithelial-mesenchymal transition and metastasis in a model of breast cancer progression. J Clin Invest **2004**;114:569-81
2. Weigelt B, Peterse JL, van 't Veer LJ. Breast cancer metastasis: markers and models. Nat Rev Cancer **2005**;5:591-602
3. Perou CM, Sorlie T, Eisen MB, van de Rijn M, Jeffrey SS, Rees CA, *et al.* Molecular portraits of human breast tumours. Nature **2000**;406:747-52
4. Almendro V, Kim HJ, Cheng YK, Gonen M, Itzkovitz S, Argani P, *et al.* Genetic and phenotypic diversity in breast tumor metastases. Cancer Res **2014**;74:1338-48
5. Trimboli AJ, Fukino K, de Bruin A, Wei G, Shen L, Tanner SM, *et al.* Direct evidence for epithelial-mesenchymal transitions in breast cancer. Cancer Res **2008**; 68:937-45
6. Thiery JP, Acloque H, Huang RY, Nieto MA. Epithelial-mesenchymal transitions in development and disease. Cell **2009**;139:871-90
7. Cano A, Perez-Moreno MA, Rodrigo I, Locascio A, Blanco MJ, del Barrio MG, *et al.* The transcription factor snail controls epithelial-mesenchymal transitions by repressing E-cadherin expression. Nat Cell Biol **2000**;2:76-83
8. Batlle E, Sancho E, Franci C, Dominguez D, Monfar M, Baulida J, *et al.* The transcription factor snail is a repressor of E-cadherin gene expression in epithelial tumour cells. Nat Cell Biol **2000**;2:84-9
9. Hajra KM, Chen DY, Fearon ER. The SLUG zinc-finger protein represses E-cadherin in breast cancer. Cancer Res **2002**;62:1613-8
10. Aigner K, Dampier B, Descovich L, Mikula M, Sultan A, Schreiber M, *et al.* The transcription factor ZEB1 (deltaEF1) promotes tumour cell dedifferentiation by repressing master regulators of epithelial polarity. Oncogene **2007**;26:6979-88
11. Comijn J, Berx G, Vermassen P, Verschueren K, van Grunsven L, Bruyneel E, *et al.* The two-handed E box binding zinc finger protein SIP1 downregulates E-cadherin and induces invasion. Mol Cell **2001**;7:1267-78
12. Yang J, Mani SA, Donaher JL, Ramaswamy S, Itzykson RA, Come C, *et al.* Twist, a master regulator of morphogenesis, plays an essential role in tumor metastasis. Cell **2004**;117:927-39
13. Tran DD, Corsa CA, Biswas H, Aft RL, Longmore GD. Temporal and spatial cooperation of Snail1 and Twist1 during epithelial-mesenchymal transition predicts for human breast cancer recurrence. Mol Cancer Res **2011**;9:1644-57
14. Moody SE, Perez D, Pan TC, Sarkisian CJ, Portocarrero CP, Sterner CJ, *et al.* The transcriptional repressor Snail promotes mammary tumor recurrence. Cancer Cell **2005**;8:197-209
15. Tran HD, Luitel K, Kim M, Zhang K, Longmore GD, Tran DD. Transient SNAIL1 expression is necessary for metastatic competence in breast cancer. Cancer Res **2014**;74:6330-40
16. Zhou BP, Deng J, Xia W, Xu J, Li YM, Gunduz M, *et al.* Dual regulation of Snail by GSK-3beta-mediated phosphorylation in control of epithelial-mesenchymal transition. Nat Cell Biol **2004**;6:931-40

17.   Zheng H, Shen M, Zha YL, Li W, Wei Y, Blanco MA*, et al.* PKD1 phosphorylation-dependent degradation of SNAIL by SCF-FBXO11 regulates epithelial-mesenchymal transition and metastasis. Cancer Cell **2014**;26:358-73

18.   Vinas-Castells R, Beltran M, Valls G, Gomez I, Garcia JM, Montserrat-Sentis B*, et al.* The hypoxia-controlled FBXL14 ubiquitin ligase targets SNAIL1 for proteasome degradation. J Biol Chem **2010**;285:3794-805

19.   Ciechanover A. The unravelling of the ubiquitin system. Nat Rev Mol Cell Biol **2015**; 16:322-4

20.   Cardozo T, Pagano M. The SCF ubiquitin ligase: insights into a molecular machine. Nat Rev Mol Cell Biol **2004**;5:739-51

21.   Wang Z, Liu P, Inuzuka H, Wei W. Roles of F-box proteins in cancer. Nat Rev Cancer **2014**;14:233-47

22.   Skaar JR, Pagan JK, Pagano M. Mechanisms and function of substrate recruitment by F-box proteins. Nat Rev Mol Cell Biol **2013**;14:369-81

23.   Tian X, Dai S, Sun J, Jin G, Jiang S, Meng F*, et al.* F-box protein FBXO22 mediates polyubiquitination and degradation of KLF4 to promote hepatocellular carcinoma progression. Oncotarget **2015**;6:22767-75

24.   Tan MK, Lim HJ, Harper JW. SCF(FBXO22) regulates histone H3 lysine 9 and 36 methylation levels by targeting histone demethylase KDM4A for ubiquitin-mediated proteasomal degradation. Mol Cell Biol **2011**;31:3687-99

25.   Johmura Y, Sun J, Kitagawa K, Nakanishi K, Kuno T, Naiki-Ito A*, et al.* SCF(Fbxo22)-KDM4A targets methylated p53 for degradation and regulates senescence. Nat Commun **2016**; 7: 10574

26.   Finn RS, Press MF, Dering J, Arbushites M, Koehler M, Oliva C*, et al.* Estrogen receptor, progesterone receptor, human epidermal growth factor receptor 2 (HER2), and epidermal growth factor receptor expression and benefit from lapatinib in a randomized trial of paclitaxel with lapatinib or placebo as first-line treatment in HER2-negative or unknown metastatic breast cancer. J Clin Oncol **2009**;27:3908-15

27.   Zlobec I, Steele R, Terracciano L, Jass JR, Lugli A. Selecting immunohistochemical cut-off scores for novel biomarkers of progression and survival in colorectal cancer. J Clin Pathol **2007**; 60: 1112-6

28.   Li DQ, Ohshiro K, Reddy SD, Pakala SB, Lee MH, Zhang Y*, et al.* E3 ubiquitin ligase COP1 regulates the stability and functions of MTA1. Proc Natl Acad Sci U S A **2009**;106:17493-8

29.   Atsumi S, Nosaka C, Adachi H, Kimura T, Kobayashi Y, Takada H*, et al.* New anti-cancer chemicals Ertredin and its derivatives, regulate oxidative phosphorylation and glycolysis and suppress sphere formation in vitro and tumor growth in EGFRvIII-transformed cells. BMC Cancer **2016**;16:496

30.   Neve RM, Chin K, Fridlyand J, Yeh J, Baehner FL, Fevr T*, et al.* A collection of breast cancer cell lines for the study of functionally distinct cancer subtypes. Cancer Cell **2006**;10:515-27

31.   Drasin DJ, Robin TP, Ford HL. Breast cancer epithelial-to-mesenchymal transition: examining the functional consequences of plasticity. Breast Cancer Res **2011**;13:226

32. Berx G, Cleton-Jansen AM, Nollet F, de Leeuw WJ, van de Vijver M, Cornelisse C, *et al.* E-cadherin is a tumour/invasion suppressor gene mutated in human lobular breast cancers. EMBO J **1995**;14:6107-15

33. Berx G, Cleton-Jansen AM, Strumane K, de Leeuw WJ, Nollet F, van Roy F, *et al.* E-cadherin is inactivated in a majority of invasive human lobular breast cancers by truncation mutations throughout its extracellular domain. Oncogene **1996**;13:1919-25

34. MacPherson MR, Molina P, Souchelnytskyi S, Wernstedt C, Martin-Perez J, Portillo F, *et al.* Phosphorylation of serine 11 and serine 92 as new positive regulators of human Snail1 function: potential involvement of casein kinase-2 and the cAMP-activated kinase protein kinase A. Mol Biol Cell **2010**;21:244-53

35. Akhoondi S, Sun D, von der Lehr N, Apostolidou S, Klotz K, Maljukova A, *et al.* FBXW7/hCDC4 is a general tumor suppressor in human cancer. Cancer Res **2007**; 67: 9006-12

36. Gstaiger M, Jordan R, Lim M, Catzavelos C, Mestan J, Slingerland J, *et al.* Skp2 is oncogenic and overexpressed in human cancers. Proc Natl Acad Sci U S A **2001**;98:5043-8

37. Zhu Q, Krakowski AR, Dunham EE, Wang L, Bandyopadhyay A, Berdeaux R, *et al.* Dual role of SnoN in mammalian tumorigenesis. Mol Cell Biol **2007**;27:324-39

38. D'Cruz CM, Gunther EJ, Boxer RB, Hartman JL, Sintasath L, Moody SE, *et al.* c-MYC induces mammary tumorigenesis by means of a preferred pathway involving spontaneous Kras2 mutations. Nat Med **2001**;7:235-9

39. Liu H, Radisky DC, Yang D, Xu R, Radisky ES, Bissell MJ, *et al.* MYC suppresses cancer metastasis by direct transcriptional silencing of alphav and beta3 integrin subunits. Nat Cell Biol **2012**;14:567-74

40. Yu ZH, Lun SM, He R, Tian HP, Huang HJ, Wang QS, *et al.* Dual function of MAZ mediated by FOXF2 in basal-like breast cancer: Promotion of proliferation and suppression of progression. Cancer Lett **2017**;402:142-52

41. Skaar JR, Pagan JK, Pagano M. SCF ubiquitin ligase-targeted therapies. Nat Rev Drug Discov **2014**;13:889-903

42. Barbash O, Zamfirova P, Lin DI, Chen X, Yang K, Nakagawa H, *et al.* Mutations in Fbx4 inhibit dimerization of the SCF(Fbx4) ligase and contribute to cyclin D1 overexpression in human cancer. Cancer Cell **2008**;14:68-78

43. Duan S, Cermak L, Pagan JK, Rossi M, Martinengo C, di Celle PF, *et al.* FBXO11 targets BCL6 for degradation and is inactivated in diffuse large B-cell lymphomas. Nature **2012**; 481:90-3

44. Wertz IE, Kusam S, Lam C, Okamoto T, Sandoval W, Anderson DJ, *et al.* Sensitivity to antitubulin chemotherapeutics is regulated by MCL1 and FBW7. Nature **2011**;471:110-4

Acknowledgements

Author contributions

RS, HYX, JXQ, YNH, FY, and FLZ performed experiments and analyzed data. ZMS and DQL supervised the entire project, designed the experiments, and analyzed data. The manuscript was written through contributions of all authors. All authors have read and approved the final manuscript.

30

Figure legends

Figure 1. FBXO22 promotes breast cancer cell proliferation *in vitro* and tumor growth *in vivo*

(A-B) Immunoblotting analysis of FBXO22 protein expression in 9 pairs of matched primary breast cancer tissues and normal breast tissue (A) and indicated cell lines (B). (C-E) MDA-MB-231 and Hs578T cells stably expressing pCDH and HA-FBXO22 (C) were subjected to cell proliferation assays using CCK-8 (D) and colony growth assays (E). Representative images of survival colonies are shown in Supplementary Figure S1D. (F-H) MCF-7 and ZR-75-1 cells stably expressing shNC and shFBXO22 (F) were subjected to cell proliferation assays using CCK-8 (G) and colony growth assays (H). Representative images of survival colonies are shown in Supplementary Figure S1H. (I-K) MDA-MB-231 cells stably expressing pCDH and HA-FBXO22 were injected into mammary fat pads of 6-week-old female BALB/c nude mice (n=8). After 8 weeks of injected, xenograft tumors were harvested. Tumor growth curves (I), photographs of harvested tumors (J), and tumor weight (K) are shown.

Figure 2. FBXO22 suppresses breast cancer cell migration, invasion, and metastasis

(A-F) MDA-MB-231 and Hs578T cells stably expressing pCDH and HA-FBXO22 were subjected to wound-healing assays (A-B), Boyden's chamber migration assays (C-D), and Matrigel-coated invasion assays (E-F). (G-J) MCF-7 and ZR-75-1 cells stably expressing shNC and shFBXO22 were analyzed by wound-healing assays (G-H), Boyden's chamber migration assays (I), and Matrigel-coated invasion assays (J). Representative images of cell migration and invasion are shown in Supplementary Figure S3E and S3F, respectively. (K-M) MDA-MB-231 cells stably expressing pCDH and HA-FBXO22 were injected into 6-week-old female BALB/c nude mice (n=6) through the tail vein. After 6 weeks of injections, the lungs were harvested. Representative images of lung metastasis (K), quantitative results of lung nodules (L), and representative images of H.E.-stained sections of lung tissues (M) are shown.

31

Figure 3. FBXO22 expression is associated with the prognosis of patients with breast cancer

(A) IHC analysis was carried out on a tissue microarray containing 164 breast cancer samples with clinical fellow-up information. Representative IHC images of FBXO22 expression are shown. (B-C) Kaplan-Meier curves of OS (B) and DFS (C) of 164 breast cancer patients with high or low FBXO22 expression.

Figure 4. FBXO22 suppresses EMT and promotes proteasomal degradation of SNAIL

(A) Immunoblotting analysis of EMT markers in MCF10A cells stably expressing pCDH and HA-FBXO22. (B) Immunofluorescence staining of E-cadherin and Vimentin in MCF10A cells stably expressing pCDH and HA-FBXO22. Cell nucleus was counterstained with DAPI. (C-D) MDA-MB-231 and Hs578T cells stably expressing pCDH and HA-FBXO22 (C) or MCF-7 and ZR-75-1 cells stably expressing shNC and shFBXO22 (D) were analyzed by immunoblotting. (E) Lysates from 4 pairs of xenograft tumors expressing pCDH and HA-FBXO22 (tumors from Figure 1J) were analyzed by immunoblotting. (F) Lysates from the indicated cell lines were analyzed by immunoblotting. (G) Cells stably expressing pCDH and HA-FBXO22 were treated with DMSO or 10 μM MG-132 for 6 h and analyzed by immunoblotting. (H-I) Cells stably expressing shNC and shFBXO22 were treated with 100 μg/mL of CHX for the indicated times and then analyzed by immunoblotting (H). Relative expression levels of SNAIL to Vinculin were shown in I. (J-K) Cells were transfected with Flag-SNAIL alone or in combination with HA-FBXO22. After 48 h of transfection, cells were subjected to immunoblotting (J) and immunofluorescent staining (K).

Figure 5. FBXO22 interacts with SNAIL and promotes its polyubiquitination

(A) Lysates from HEK293T cells transfected with Flag-SNAIL were incubated with bacterially expressed GST or GST-FBXO22 protein for 2 h. GST pull-down proteins were analyzed by

32

immunoblotting with an anti-Flag antibody. GST or GST-FBXO22 protein was visualized by Ponceau S staining. (B) Lysates from HEK293T cells transfected with HA-FBXO22 were incubated with GST or GST-SNAIL protein for 2 h. GST pull-down proteins were analyzed by immunoblotting with an anti-HA antibody. GST or GST-SNAIL protein was visualized by Ponceau S staining. (C) HEK293T cells were transfected with Flag-SNAIL and HA-FBXO22 alone or in combination. After 48 h of transfection, cells were treated with 20 μM MG-132 for 6 h and subjected to sequential IP-immunoblotting analyses. (D) Lysates from ZR-75-1 and T47D cells were immunoprecipitated with control IgG or an anti-SNAIL antibody, followed by immunoblotting analysis. (E-F) GST pull-down assays were performed using exogenously expressed Flag-SNAIL and purified GST or GST-FBXO22 proteins. (G-H) HEK293T cells were transfected with the indicated expression vectors. After 48 h of transfection, cells were treated with 20 μM MG-132 for 6 h. Lysates were subjected to IP analysis under the native (G) or denaturing (H) conditions, followed by immunoblotting analysis. (I-J) MDA-MB-231 cells stably expressing pCDH and HA-FBXO22 (I) or MCF-7 cells stably expressing shNC and shFBXO22 (J) were treated with 10 μM of MG-132 for 6 h and subjected to the sequential IP-immunoblotting analysis. (K) *In vitro* ubiquitination assays were performed using the purified intact HA-FBXO22 E3 ligase complex and Flag-SNAIL from HEK293T cells in the presence of Ubiquitin, E1, E2 (UbcH5a), and ATP.

Figure 6. GSK3β phosphorylation is required for ubiquitin-dependent proteasomal degradation of SNAIL by FBXO22

(A-B) MDA-MB-231 cells stably expressing pCDH and HA-FBXO22 (A) or MCF-7 cells stably expressing shNC and shFBXO22 (B) were treated with or without 10 μM GSK3β inhibitor CHIR-99021, 10 μM PKA inhibitor H89, and 10 μM PKD1 inhibitor CID755673 for 24 h and subjected to immunoblotting analysis. (C) HEK293T cells were transfected with the indicated expression vectors. After 48 h of transfection, cells were treated with or without 10 μM CHIR-99021 for 24 h

33

and subjected to sequential IP-immunoblotting analysis. (D) HEK293T cells were transfected with the indicated expression vectors. After 48 h of transfection, cells were subjected to sequential IP-immunoblotting analysis. (E) HEK293T cells were transfected with the indicated expression vectors and analyzed by immunoblotting after 48 h of transfection. (F-G) HEK293T cells were transfected with the indicated expression plasmids. After 48 h of transfection, cells were treated with 100 µg/ml of CHX for the indicated times and analyzed by immunoblotting (F). The relative expression levels of Flag-SNAIL to Vinculin are shown in G. (H-I) MDA-MB-231 cells stably expressing pCDH, HA-FBXO22 alone or in combination with either Flag-SNAIL or Flag-SNAIL S4A were subjected to Boyden's chamber migration assays and Matrigel-coated invasion assays (H). The corresponding quantitative results are shown in I.

Figure 7. Patient-derived W52R mutation abrogates the ability of FBXO22 to degrade SNAIL and to suppress cell migration, invasion, and metastasis

(A) HEK293T cells were transfected with the indicated express constructs. After 48 h of transfection, cells were harvested for sequential IP-immunoblotting analysis. (B) MDA-MB-231 cells stably expressing pCDH, HA-FBXO22, HA-FBXO22 ΔF, or HA-FBXO22 W52R were analyzed by immunoblotting. (C-D) HEK293T cells were transfected with the indicated expression vectors. After 48 h of transfection, cells were treated with 10 µM MG-132 for 6 h and subjected to sequential IP-immunoblotting analysis. (E) HEK293T cells were transfected with the indicated expression plasmids. After 48 h of transfection, cells were treated with 100 µg/ml of CHX for the indicated times and then analyzed by immunoblotting analysis. The relative SNAIL expression levels (SNAIL/Vinculin) are shown in Supplementary Figure S9B. (F-G) MDA-MB-231 cells stably expressing pCDH, HA-FBXO22, HA-FBXO22 ΔF, HA-FBXO22 W52R were subjected to migration and invasion assays as described above. (H-J) MDA-MB-231 cells stably expressing pCDH, HA-FBXO22, HA-FBXO22 ΔF-box, and HA-FBXO22 W52R were injected

into 6-week-old female BALB/c nude mice (n=6) through the tail vein. The lungs were harvested

after 6 weeks of injection. Representative images of lung metastasis (H), quantitative results of

lung nodules (I), and representative images of H.E.-stained sections of lung tissues (J) are
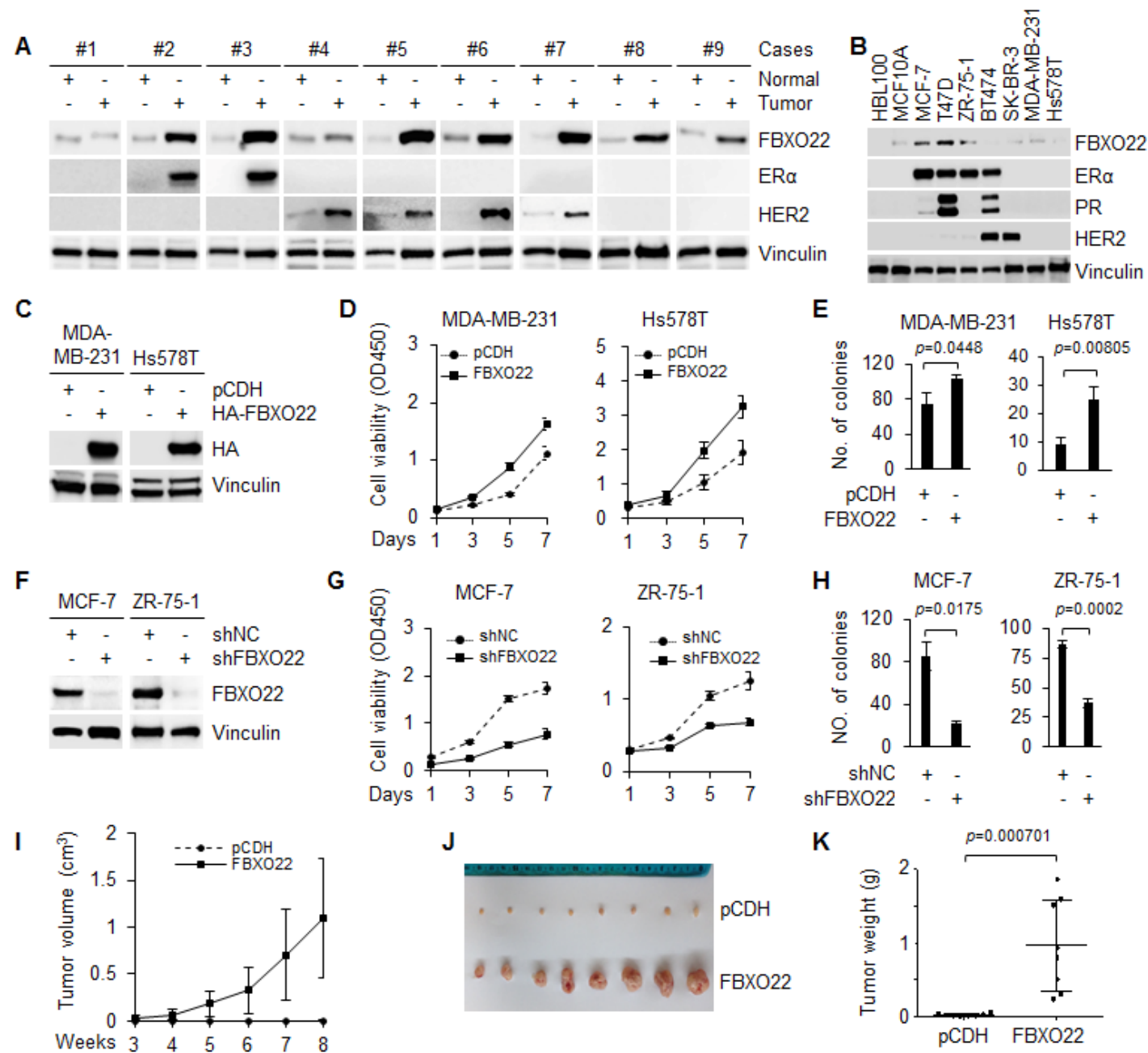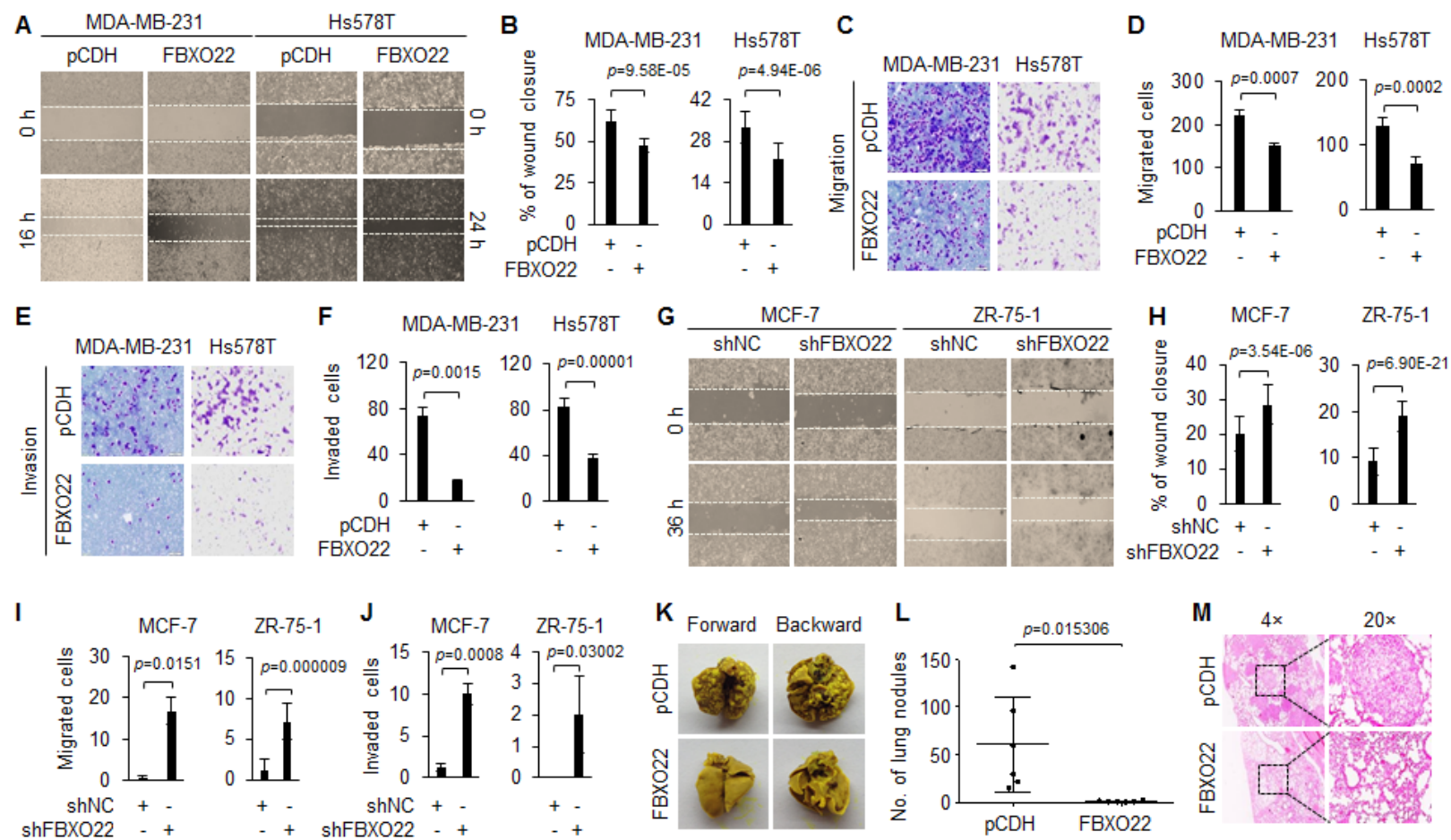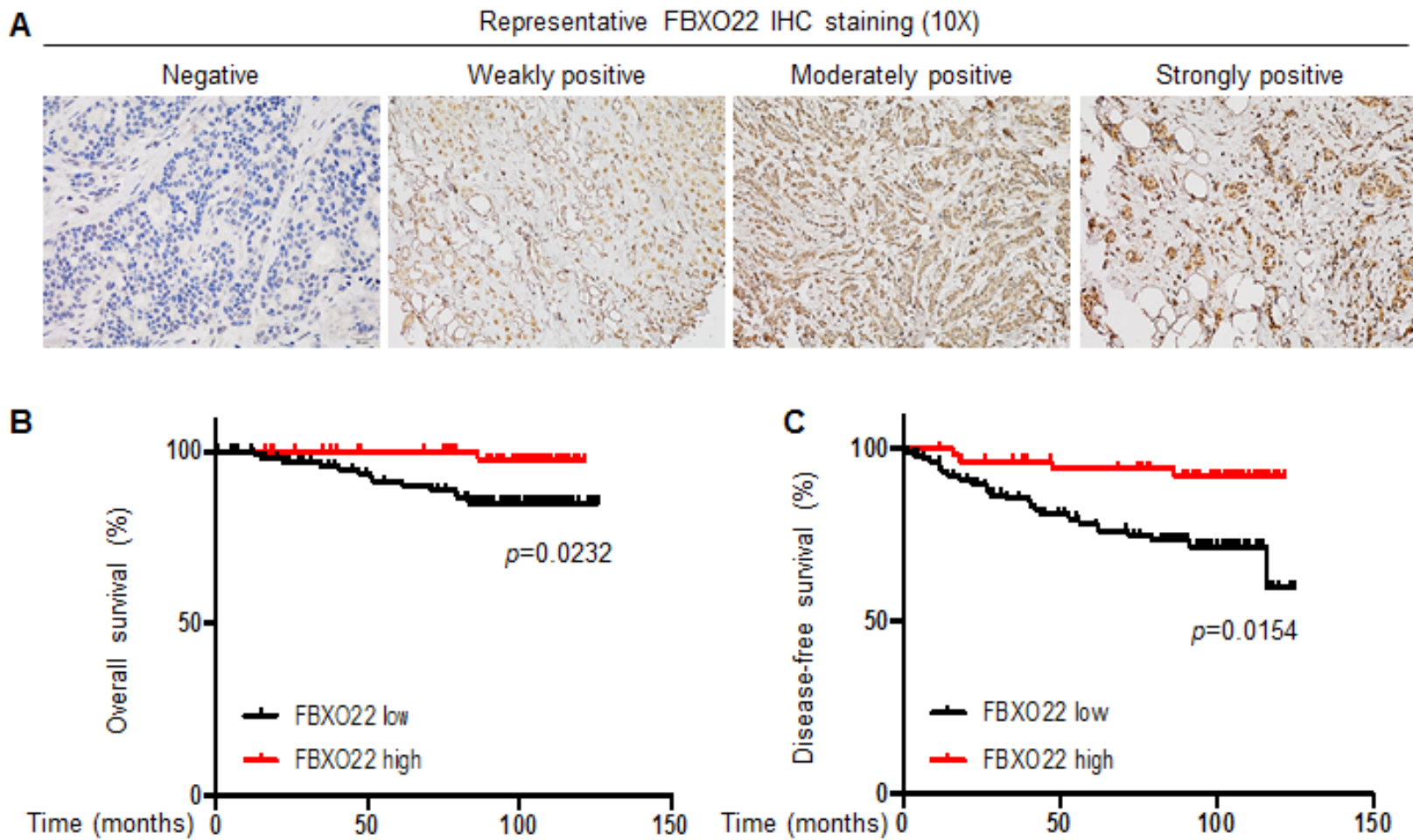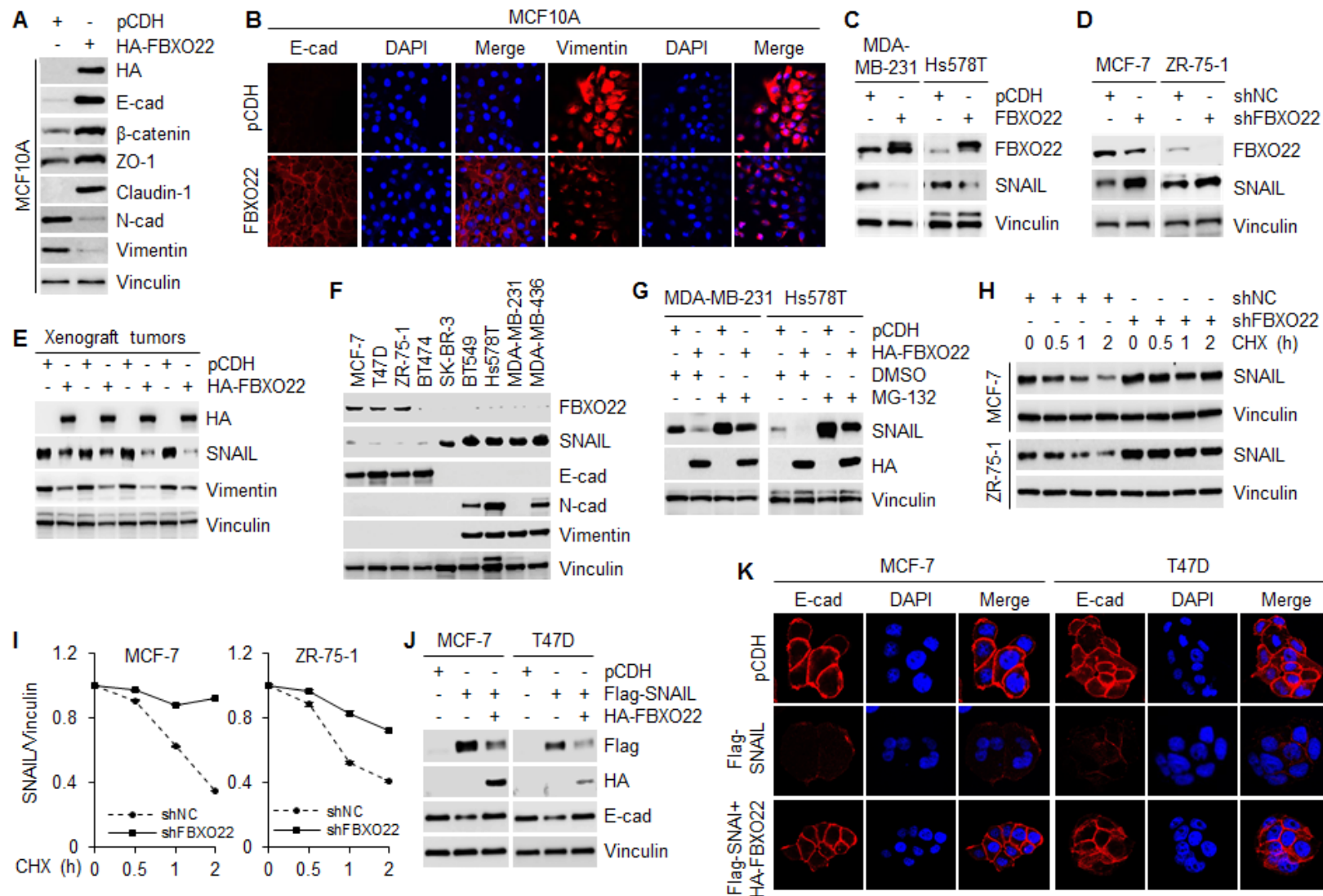
shown.

35

Figure 1

Figure 2

A   Representative FBXO22 IHC staining (10X)

Negative   Weakly positive   Moderately positive   Strongly positive

B

Overall survival (%)

$p=0.0232$

FBXO22 low
FBXO22 high

Time (months)

C

Disease-free survival (%)

$p=0.0154$

FBXO22 low
FBXO22 high

Time (months)
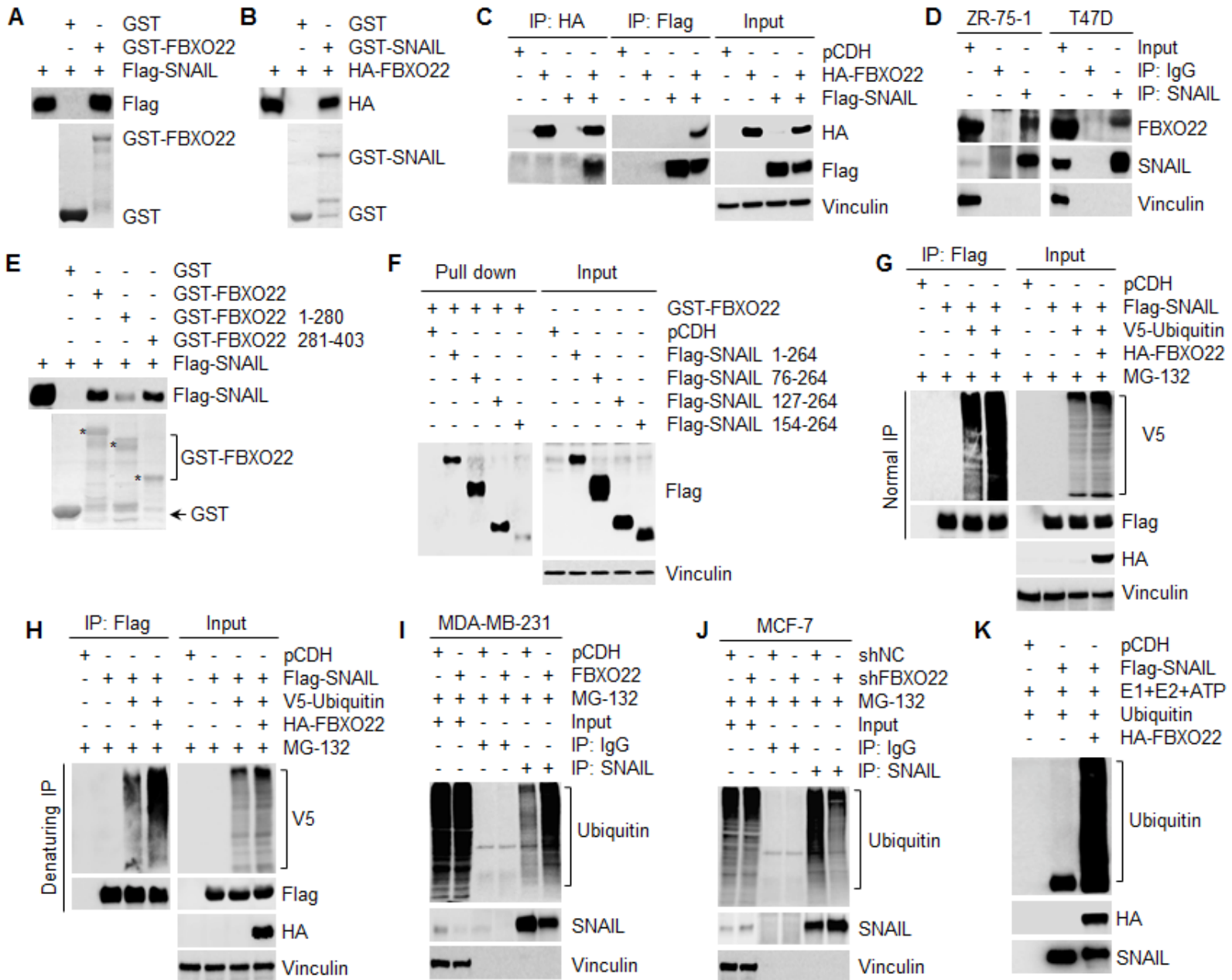
Figure 3

Figure 4

Figure 5
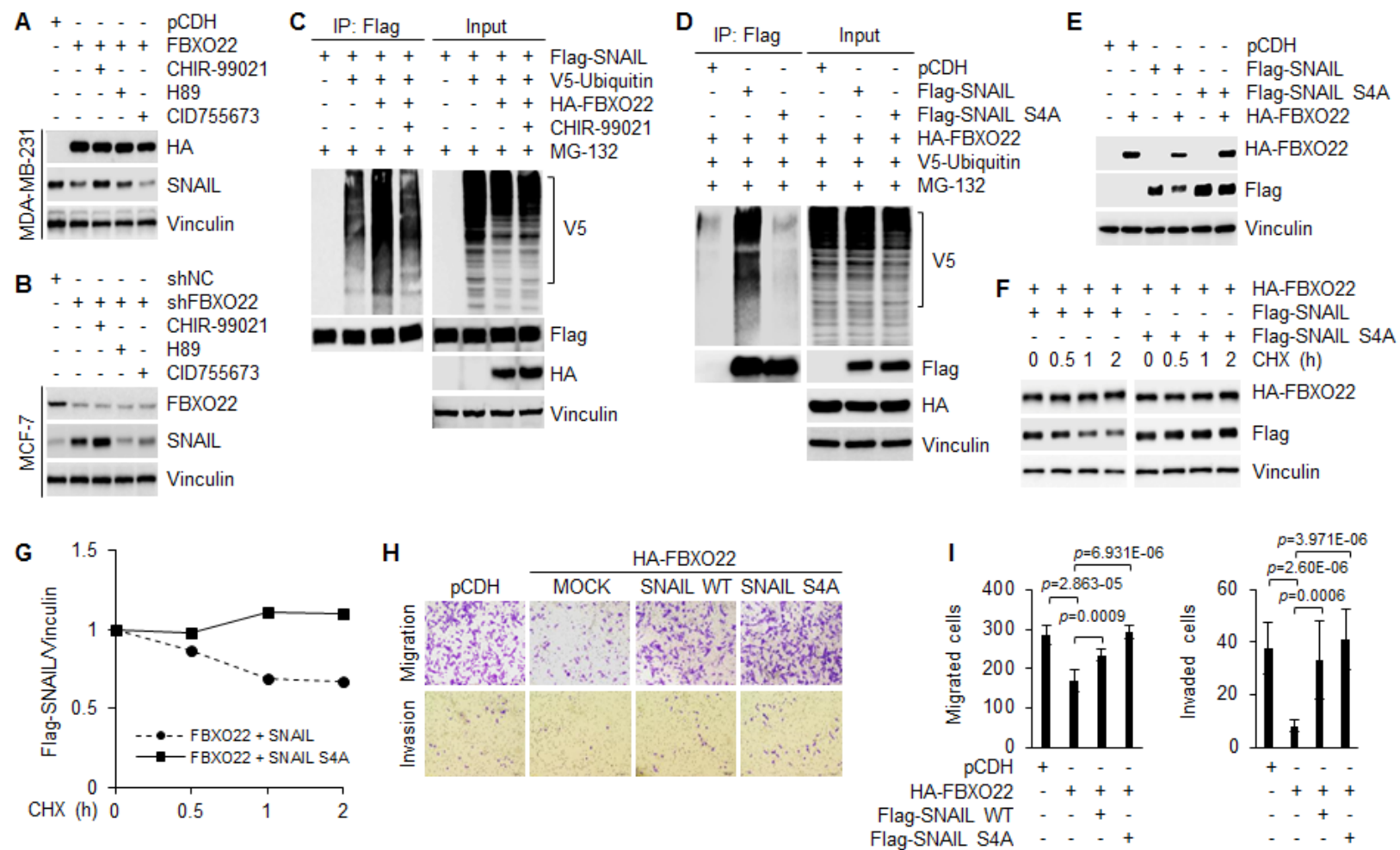
Figure 6
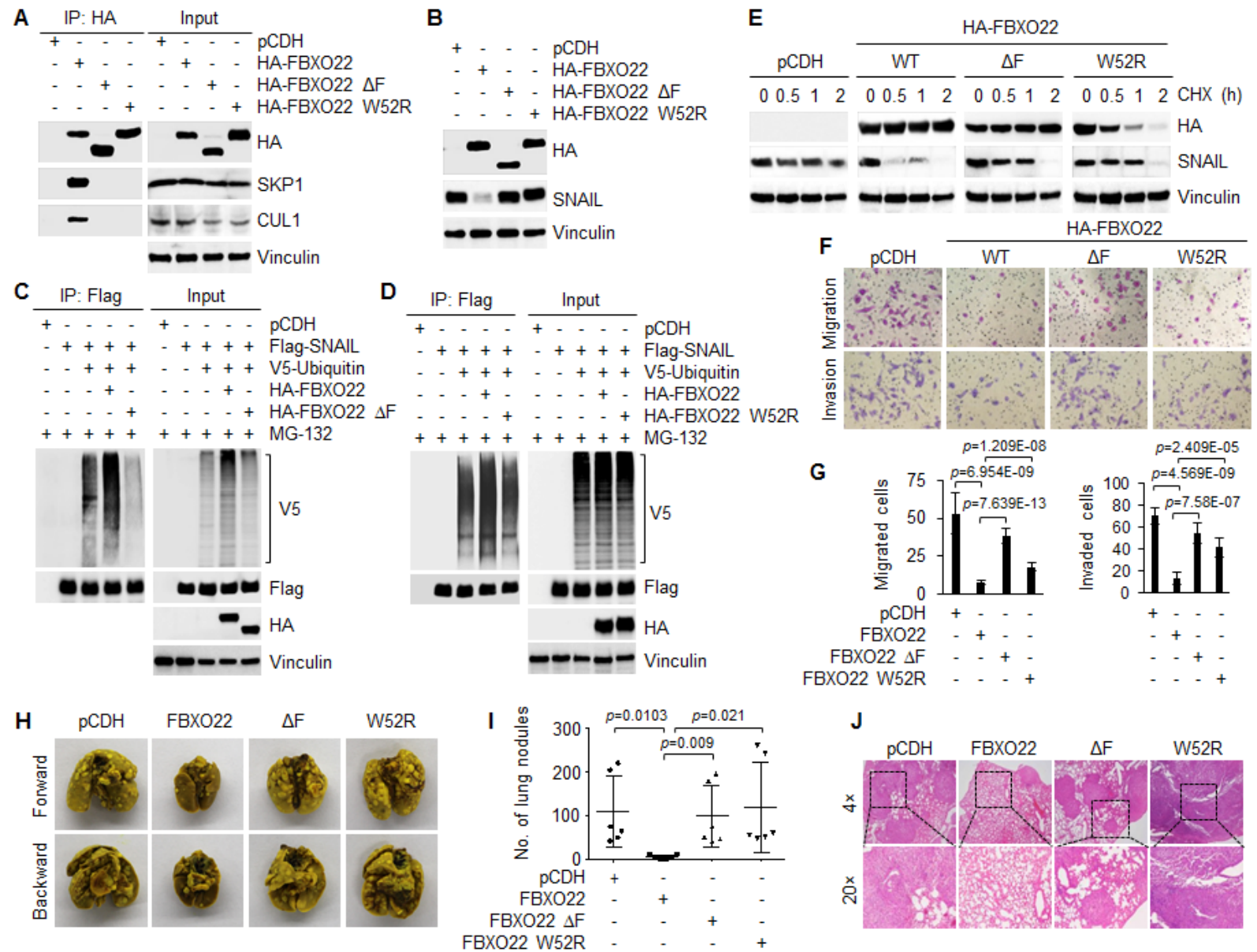
Figure 7

Cancer Research

The Journal of Cancer Research (1916–1930) | The American Journal of Cancer (1931–1940)

AACR American Association for Cancer Research

FBXO22 possesses both pro-tumorigenic and anti-metastatic roles in breast cancer progression

Rui Sun, Hong-Yan Xie, Jin-Xian Qian, et al.

Cancer Res Published OnlineFirst June 26, 2018.

E-mail alerts	Sign up to receive free email-alerts related to this article or journal.
Reprints and Subscriptions	To order reprints of this article or to subscribe to the journal, contact the AACR Publications Department at pubs@aacr.org.
Permissions	To request permission to re-use all or part of this article, use this link http://cancerres.aacrjournals.org/content/early/2018/06/26/0008-5472.CAN-17-3647. Click on "Request Permissions" which will take you to the Copyright Clearance Center's (CCC) Rightslink site.